Available online at www.sciencedirect.com
ScienceDirect
Journal of Sound and Vibration 307 (2007) 89–112
JOURNAL OF SOUND AND VIBRATION
www.elsevier.com/locate/jsvi

Stability and natural frequencies of a weakened Timoshenko beam-column with generalized end conditions under constant axial load

Luis G. Arboleda-Monsalve[a,*,1], David G. Zapata-Medina[b,2], J. Dario Aristizabal-Ochoa[c]

[a]*School of Civil Engineering, Purdue University, West Lafayette, IN, USA*
[b]*University of Kentucky, Lexington, KY, USA*
[c]*125-year Generation Professor, School of Mines, National University, Colombia*

Received 30 September 2005; received in revised form 11 October 2006; accepted 15 June 2007

Abstract

The stability and free vibration analyses of a Timoshenko beam-column with generalized end conditions (i.e., with semi-rigid flexural connections and lateral bracings at both ends) subjected to constant axial load (tension or compression), and weakened by a cracked section along its span are presented. The magnitude and location of the weakened section are both arbitrary and independent of each other. The magnitude of the crack is modeled as an intermediate flexural connection of zero length producing a member with two-segments with rotational discontinuity at the weakened section but of identical lateral deflection. The proposed model offers the option of considering the beneficial effects of an additional lateral bracing located at the weakened section to alleviate the detrimental effects of the rotational discontinuity on the stability and natural frequencies of the whole beam-column. The proposed model includes the following coupling effects: (1) shear and bending deformations along the member's span; (2) the translational and rotational masses of the member uniformly distributed along its span; (3) constant axial load (tension or compression) applied at both ends; and (4) the shear forces along the member induced by the applied axial load as the beam-column deforms according to two different approaches: proportional to the bending rotation or to the total slope of the member axis. A flowchart is included that shows the steps necessary to carry out the stability and free vibration analyses. Finally, to show the validity and simplicity of the proposed method and equations five comprehensive examples are presented using the two approaches of the induced shear force and the obtained results are compared to those calculated by other analytical methods including the finite element method.

*Corresponding author. Tel.: +1 765 4092135; fax: +1 317 2598262.
E-mail address: larboleda@jsengr.com (L.G. Arboleda-Monsalve).
[1]Project Engineer, Janssen and Spaans Engineering Inc., Indianapolis, IN, 46216; formerly, Graduate Student, Purdue University, West Lafayette, IN, USA.
[2]Graduate Student, Department of Civil and Environmental Engineering, Northwestern University, Evanston, IL 60208, USA.

0022-460X/$ - see front matter © 2007 Elsevier Ltd. All rights reserved.
doi:10.1016/j.jsv.2007.06.059

Nomenclature

A	cross sectional area of the beam-column
A_s	effective area for shear of the beam-column ($=kA$)
$C_1,C_2,C_3,C_4,C_5,C_6,C_7,C_8$	constants required in the modal shapes
E	elastic modulus of the material
f	natural frequency of the beam-column (Hz)
G	shear modulus of the material
I	moment of inertia of the beam-column cross section
K	effective shear factor of the beam-column cross section ($=A_s/A$)
κ_a, κ_b and κ_c	stiffness of the flexural connections at A, B and C, respectively (force–distance/rad)
L	beam-column span
$\bar{m}$	mass per unit length of the beam-column ($=\rho A$)
M	bending moment
P	compressive axial load applied at the ends of the beam-column
r	radius of gyration of the beam cross section
R	slenderness parameter ($=r/L$)
R_a, R_b and R_c	stiffness indices of the flexural connections at A, B and C, respectively
S_a, S_b and S_c	stiffness indices of the lateral bracings at A, B and C of the beam-column, respectively
t	time
V	shear force
x	coordinate along the centroidal axis of the beam-column
y	total lateral deflection of the centroidal line of the beam-column
$Y(x)$	shape function of the total lateral deflection of the centroidal line of the beam-column
γ	shear distortion
$\Theta(x)$	shape function of the slope of the centroidal line of the beam-column due to bending only
θ	slope, due to bending of the centroidal line of the beam-column
ξ	ratio of the crack depth to the height of the rectangular cross section
ρ	mass per unit volume (density) of the material of the beam-column
ω	natural angular frequency of the beam-column (rad/s)

1. Introduction

The effects of flexural cracking on the static and dynamic response of beams and beam-columns are of great importance in earthquake, mechanical, bridge, and structural engineering. The stability and vibration of beam-columns with a weakened cross section along the span has been extensively investigated by several researchers. Anifantis and Dimarogonas [1] developed a general flexibility matrix to study the stability of columns with a single edge crack subjected to follower forces. Cheng and Pantelides [2] studied the dynamic behavior of Timoshenko beam-columns on elastic foundation with emphasis on the two approaches used in this publication. Dimarogonas [3] presented the state-of-the-art review with over 500 references related to crack effects on the dynamics of framed structures. Chondros et al. [4] and Chondros [5] analyzed the stress field changes in the vicinity of the crack location using fracture mechanics methods. The changes in the stress, strain and displacement distributions due to the crack were incorporated using a crack disturbance function. The effect of the flexibility due to the crack was distributed along the length of the beam. Several comparisons were made between the lumped crack flexibility and the continuous flexibility approach and the results were matched with experimental results in aluminum beams tested in the University of Patras, Greece. Takahashi [6] analyzed the static and vibration of non-uniform Timoshenko beams using the transfer matrix method. Panteliou et al. [7] proposed a crack identification method based on the thermodynamic theory of damping. They investigated analytically and experimentally the behavior of a homogeneous, isotropic, and elastic bar with a single-edge surface crack. They found a correlation between the depth of crack and the damping factor. Shifrin and Ruotolo [8] proposed a technique for calculating the natural frequencies of Euler–Bernoulli beams

with an arbitrary number of cracks. Li [9–11] studied the buckling and vibration of stepped columns with arbitrary number of cracks including the shear deformation effects. Wang et al. [12] presented, using the Engesser's model, the buckling loads of a Timoshenko column under intermediate and concentrated loads and studied the shear deformation effects. Recently, Aristizabal-Ochoa [13] studied the influence of the shearing forces and deformations on the static stability of Timoshenko beam-columns. Lee et al. [14] studied the effects of an internal hinge along the span on the dynamic characteristics of clamped–clamped and clamped–pinned Timoshenko beams including criteria to determine its optimal location for maximum natural frequency. Fan and Zheng [15] studied the effects of multiple cracks on the stability of Timoshenko beam-columns based on modified Fourier series. Chandra Kishen and Kumar [16] studied the buckling of cracked beam-columns under eccentric axial loads using the finite element method. More recently, Wang et al. [17] studied the buckling of a single cracked column according to Euler theory with different end conditions (i.e., free, perfectly hinged, and clamped). Finally, Binici [18] studied the effect of the crack location on the natural frequencies and modal shapes of an Euler–Bernoulli beam containing multiple cracks under constant axial force. There are numerous analytical and experimental studies that deal with the static and dynamic behavior of beam-columns. Unfortunately, due to space limitations it is not feasible to present herein a complete list of references related to this subject.

On the other hand, there is not a single study on the static and dynamic stability of weakened Timoshenko beam-columns with generalized end conditions that includes the combined effects of bending and shear deformations, rotational and translational inertias of the member, and the shear component induced by the applied axial force as the member deforms. Therefore, the main objectives of this publication are: (1) to present a complete classical formulation on this subject; (2) to provide a practical approach to determine the critical loads, natural frequencies, and the corresponding modes of a weakened Timoshenko beam-column with generalized end conditions; and (3) to compare both the natural frequencies and buckling loads of slender and short beam-columns obtained using different theories such as those by Bernoulli–Euler, Rayleigh, Shear Beam, and Timoshenko. This paper is an extension of the Timoshenko beam-column with generalized end conditions recently presented by Aristizabal-Ochoa [19] but it includes the detrimental effects of a single weakened section and the beneficial effects of a lateral bracing located at the discontinuity. Five comprehensive examples are presented and the obtained results compared to those obtained using other methods to show: (1) the simplicity of the proposed model and corresponding equations; (2) the detrimental effects of the magnitude and location of a crack; and (3) the effects of the shear force induced by the applied axial load using two approaches (proportional to the bending rotation or to the total slope of the member axis as proposed by Timoshenko and Gere [20]).

2. Structural model

Consider the beam-column ACB (shown in Fig. 1a) made of two segments AC and CB, end connections κ_a and κ_b, and lateral springs or bracings S_a and S_b (whose dimensions are in force/distance) at extremes A and B, respectively. The crack located at C at a distance a from end A is simulated with a concentrated flexural spring κ_c. To study the effects of lateral bracing at the crack location C, the bracing S_c is included. The ratios $R_a = \kappa_a/(EI/L)$, $R_b = \kappa_b/(EI/L)$, and $R_c = \kappa_c/(EI/L)$ are denoted as the flexural stiffness indices of the flexural connections at A, B, and C, respectively. In addition, the ratios $\bar{S}_a = S_a/(A_sG/L)$, $\bar{S}_b = S_b/(A_sG/L)$, and $\bar{S}_c = S_c/(A_sG/L)$ are denoted as the shear stiffness indices of the lateral bracings at A, B, and C, respectively. The indices R_a, R_b, $\bar{S}_a$ and $\bar{S}_b$ allow the analyst to simulate any end support conditions applied to the beam-column ACB, and R_c to simulate the magnitude of the flexural crack.

The flexural stiffness indices R_a and R_b can vary from zero (for perfectly hinged ends) to infinity (for perfectly clamped ends), whereas R_c can vary from zero (for a perfectly hinge with zero moment capacity, and consequently discontinuous slope in the member at C) to infinity (for a perfectly uncracked section, and consequently with continuous slope at C). The shear stiffness indices $\bar{S}_a$ and $\bar{S}_b$ also vary from zero (for unbraced ends) to infinity (for fully braced ends with zero lateral displacement). Values of these indices between zero and infinity represent semi-rigid flexural connections and partially braced lateral conditions, respectively.

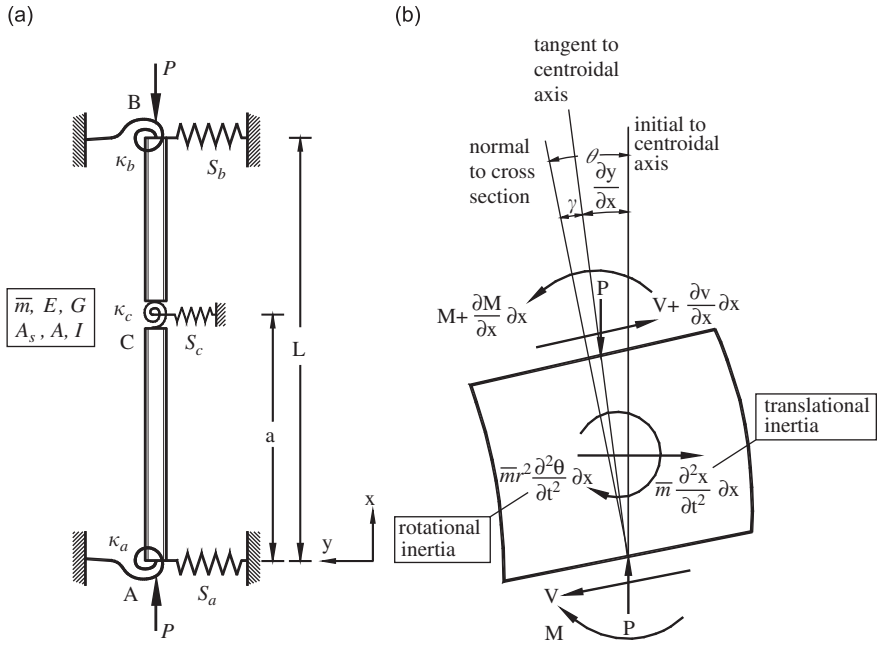

Fig. 1. Structural model: (a) connections and properties of the two-segment beam-column and (b) differential element (forces, moments and deformations).

It is assumed that the beam-column ACB: (1) is made of a homogenous linear elastic material with moduli E and G; (2) its centroidal axis is a straight line; (3) is loaded axially at the ends along its centroidal x-axis with a constant load P (tension or compression); (4) its transverse cross section is doubly symmetric (i.e., its centroid coincides with the shear center) with a total area A, an effective shear area A_s and a principal moment of inertia $I = Ar^2$ about the plane of bending (r = radius of gyration of the cross section); (5) with a uniform mass per unit of length $\bar{m} = \rho A$ (ρ = density of the material); and (6) all transverse deflections, rotations, and strains along the beam are small, so that the principle of superposition is applicable.

3. Governing equations and general solution

The transverse and bending equations of equilibrium of the Timoshenko beam-column differential element shown in Fig. 1b are the following:

$$\frac{\partial V}{\partial x} = -\bar{m}\frac{\partial^2 y}{\partial t^2}, \tag{1}$$

$$\frac{\partial M}{\partial x} = V + \bar{m}r^2\frac{\partial^2\theta}{\partial t^2} - P\frac{\partial y}{\partial x}. \tag{2}$$

The effects of the shear forces along the member induced by the applied axial load as the member deforms and deflects are taken into account according to two different approaches: proportional to the bending rotation θ or to the total slope of the member axis $\partial y/\partial x$ as proposed by Timoshenko and Gere [20].

3.1. Shear component proportional to bending rotation θ

Assuming that

$$V = A_s G\gamma + P\theta \tag{3}$$

and knowing that: $M = EI\partial\theta/\partial x$, $\gamma = \theta - (\partial y/\partial x)$, and that E, G, I, A, A_s, $\bar{m}$, and P remain constant along of the member, Eqs. (1) and (2) become

$$A_sG\left(\frac{\partial\theta}{\partial x} - \frac{\partial^2 y}{\partial x^2}\right) + P\frac{\partial\theta}{\partial x} + \bar{m}\frac{\partial^2 y}{\partial t^2} = 0, \tag{4}$$

$$EI\frac{\partial^2\theta}{\partial x^2} - A_sG\left(\theta - \frac{\partial y}{\partial x}\right) - P\theta - \bar{m}r^2\frac{\partial^2\theta}{\partial t^2} + P\frac{\partial y}{\partial x} = 0. \tag{5}$$

Using separation of variables, the solutions to Eqs. (4) and (5) are: $y(x,t) = Y(x)\sin(\omega t)$ and $\theta(x,t) = \Theta(x)\sin(\omega t)$, respectively. Substituting these solutions into Eqs. (4) and (5), they become:

$$A_sG\left(\frac{\mathrm{d}\Theta}{\mathrm{d}x} - \frac{\mathrm{d}^2 Y}{\mathrm{d}x^2}\right) + P\frac{\mathrm{d}\Theta}{\mathrm{d}x} - \bar{m}\omega^2 Y = 0, \tag{6}$$

$$EI\frac{\mathrm{d}^2\Theta}{\mathrm{d}x^2} - A_sG\left(\Theta - \frac{\mathrm{d}Y}{\mathrm{d}x}\right) - P\Theta + P\frac{\mathrm{d}Y}{\mathrm{d}x} + \bar{m}r^2\omega^2\Theta = 0. \tag{7}$$

Eqs. (6) and (7) are coupled together in $Y(x)$ and $\Theta(x)$ which represent the shape functions or the proper functions associated with the lateral deflection and the section rotation along the member, respectively.

The stability and free vibration analyses of a Timoshenko beam-column with a single weakened section depend on 15 variables: E, G, L, a, P, $\bar{m}$, ω, r, A_s, κ_a, κ_b, κ_c, S_a, S_b, and S_c. However, these variables can be grouped into the following 10 dimensionless parameters and indices: $b^2 = (\bar{m}\omega^2)/(EI/L^4)$ (frequency parameter); $s^2 = (EI/L^2)/A_sG$ (bending-to-shear stiffness parameter); $F^2 = P/(EI/L^2)$ (axial-load parameter); $R^2 = r^2/L^2$ (slenderness parameter); $R_a = \kappa_a/(EI/L)$, $R_b = \kappa_b/(EI/L)$ and $R_c = \kappa_c/(EI/L)$ (flexural-stiffness indices at extremes A and B, and at the weakened section C, respectively); $\bar{S}_a = S_a/(A_sG/L)$, $\bar{S}_b = S_b/(A_sG/L)$ and $\bar{S}_c = S_c/(A_sG/L)$ (lateral shear-stiffness indices or bracings indices at extremes A and B, and at the weakened section C, respectively).

Eqs. (6) and (7) when expressed in terms of the aforementioned parameters and indices are reduced to:

$$(1 + F^2s^2)\frac{\mathrm{d}\Theta}{\mathrm{d}\bar{x}} - \frac{\mathrm{d}^2\bar{Y}}{\mathrm{d}\bar{x}^2} - b^2s^2\bar{Y} = 0, \tag{8}$$

$$s^2\frac{\mathrm{d}^2\Theta}{\mathrm{d}\bar{x}^2} - (1 + F^2s^2 - b^2s^2R^2)\Theta + (1 + F^2s^2)\frac{\mathrm{d}\bar{Y}}{\mathrm{d}\bar{x}} = 0, \tag{9}$$

where $\bar{x} = x/L$ and $\bar{Y} = Y/L$.

The second-order differential Eqs. (8) and (9), which are coupled together, can be further reduced by eliminating Θ to the following single fourth-order differential equation:

$$\frac{\mathrm{d}^4\bar{Y}}{\mathrm{d}\bar{x}^4} + 2\Omega\frac{\mathrm{d}^2\bar{Y}}{\mathrm{d}\bar{x}^2} + \varepsilon\bar{Y} = 0, \tag{10}$$

where

$$\Omega = (b^2s^2 + b^2R^2 + F^2 + F^4s^2)/2 \tag{11}$$

and

$$\varepsilon = b^4R^2s^2 - b^2 - b^2F^2s^2. \tag{12}$$

The solution to Eq. (10) is of the form

$$\bar{Y}(\bar{x}) = c\,\mathrm{e}^{m\bar{x}}. \tag{13}$$

After substituting Eq. (13) into the governing Eq. (10), the following algebraic expression is obtained: $m^4 + 2\Omega m^2 + \varepsilon = 0$, whose solutions are: $m = \pm\sqrt{-\Omega - \sqrt{\Omega^2 - \varepsilon}}$ and $m = \pm\sqrt{-\Omega + \sqrt{\Omega^2 - \varepsilon}}$ or $m = \pm i\beta,\ \pm\alpha$, where

$$\beta = \sqrt{\Omega + \sqrt{\Omega^2 - \varepsilon}} \tag{14}$$

and

$$\alpha = \sqrt{-\Omega + \sqrt{\Omega^2 - \varepsilon}}. \tag{15}$$

Therefore the following transfer functions are obtained from the above equations:

$$\bar{Y} = C_1 \sin(\beta\bar{x}) + C_2 \cos(\beta\bar{x}) + C_3 \sinh(\alpha\bar{x}) + C_4 \cosh(\alpha\bar{x}), \tag{16}$$

$$\Theta = \lambda C_1 \cos(\beta\bar{x}) - \lambda C_2 \sin(\beta\bar{x}) + \delta C_3 \cosh(\alpha\bar{x}) + \delta C_4 \sinh(\alpha\bar{x}), \tag{17}$$

$$\bar{V} = -\frac{b^2 s^2}{\beta} C_1 \cos(\beta\bar{x}) + \frac{b^2 s^2}{\beta} C_2 \sin(\beta\bar{x}) + \frac{b^2 s^2}{\alpha} C_3 \cosh(\alpha\bar{x}) + \frac{b^2 s^2}{\alpha} C_4 \sinh(\alpha\bar{x}), \tag{18}$$

$$\bar{M} = -\lambda\beta C_1 \sin(\beta\bar{x}) - \lambda\beta C_2 \cos(\beta\bar{x}) + \delta\alpha C_3 \sinh(\alpha\bar{x}) + \delta\alpha C_4 \cosh(\alpha\bar{x}), \tag{19}$$

where

$$\lambda = \frac{\beta^2 - b^2 s^2}{\beta(1 + F^2 s^2)}, \tag{20}$$

$$\delta = \frac{\alpha^2 + b^2 s^2}{\alpha(1 + F^2 s^2)} \tag{21}$$

and C_1, C_2, C_3, and C_4 = constants determined using boundary conditions.

Note: If $\varepsilon > 0$ the following changes must be made in Eqs. (16)–(21): α for $i\alpha$; $\sin\alpha$ for $\sinh\alpha$; and $\cos\alpha$ for $\cosh\alpha$ (where $i = \sqrt{-1}$). These solutions are identical to those presented by Karnovsky and Lebed [21].

3.2. Shear component proportional to the total slope $\partial y/\partial x$

Assuming that

$$V = A_s G\gamma + P\frac{\partial y}{\partial x} \tag{22}$$

and knowing that $M = EI\partial\theta/\partial x$, $\gamma = \theta - (\partial y/\partial x)$, and that E, G, I, A, A_s, $\bar{m}$, and P remain constant along of the member, Eqs. (1) and (2) become

$$A_s G\left(\frac{\partial\theta}{\partial x} - \frac{\partial^2 y}{\partial x^2}\right) + P\frac{\partial^2 y}{\partial x^2} + \bar{m}\frac{\partial^2 y}{\partial t^2} = 0, \tag{23}$$

$$EI\frac{\partial^2\theta}{\partial x^2} - A_s G\left(\theta - \frac{\partial y}{\partial x}\right) - \bar{m}r^2\frac{\partial^2\theta}{\partial t^2} = 0. \tag{24}$$

Eqs. (23) and (24) lead to the Engesser's formula [22] which is cited by Timoshenko and Gere [20] (p. 133). Using separation of variables in the same way as in the first approach, Eqs. (23) and (24) are reduced to

$$A_s G\left(\frac{d\Theta}{dx} - \frac{d^2 Y}{dx^2}\right) + P\frac{d^2 Y}{dx^2} - \bar{m}\omega^2 Y = 0, \tag{25}$$

$$EI\frac{d^2\Theta}{dx^2} - A_sG\left(\Theta - \frac{dY}{dx}\right) + \bar{m}r^2\omega^2\Theta = 0. \tag{26}$$

Introducing the aforementioned dimensionless parameters and indices, Eqs. (25) and (26) become

$$\frac{d\Theta}{d\bar{x}} - (1 - F^2s^2)\frac{d^2\bar{Y}}{d\bar{x}^2} - b^2s^2\bar{Y} = 0, \tag{27}$$

$$s^2\frac{d^2\Theta}{d\bar{x}^2} - \frac{d\bar{Y}}{d\bar{x}} + (b^2s^2R^2 - 1)\Theta = 0. \tag{28}$$

Note that by eliminating Θ in Eqs. (27) and (28), the fourth-order differential Eq. (10) can be obtained. The solution and the corresponding transfer functions have the same form as Eqs. (16)–(19). However, Ω, ε, δ, and λ must be exchanged for the following expressions:

$$\Omega = \frac{b^2s^2 + b^2R^2 + F^2 - b^2R^2s^2F^2}{2(1 - F^2s^2)}, \tag{29}$$

$$\varepsilon = \frac{b^4R^2s^2 - b^2}{1 - F^2s^2}, \tag{30}$$

$$\lambda = \frac{(1 - F^2s^2)\beta^2 - b^2s^2}{\beta}, \tag{31}$$

$$\delta = \frac{(1 - F^2s^2)\alpha^2 + b^2s^2}{\alpha}. \tag{32}$$

3.3. Crack model on a Timoshenko beam-column

The crack is modeled as a local flexibility in an arbitrary location of the member and it is assumed that affects only the close vicinity of such location. Therefore, a rotational discontinuity in the member can be modeled as a torsional spring of local flexibility κ_c (force–distance/rad, κ_c) and calculated using the fracture mechanics approach. Chondros [5] presented an expression for a single-sided open crack in rectangular beams. Zheng and Fan [23] presented formulas ready to use not only for rectangular and circular-solid-sectional beams, but also for rectangular and circular-hollow-sectional beams taking into account shallow cracks (those whose penetration depth is in the solid region only) and deeper cracks (in which the crack goes into the middle hollow-sectional region). Technical literature about the flexibility function induced by the crack is extensively available in most international publications; nonetheless, due to space limitations this paper only considers a particular case: open cracks. For instance, the case of a crack that opens and closes due to vibration (breathing cracks [5]) is out of the scope of this paper. Then, the cracked member is modeled by two Timoshenko beam-column segments as shown by Fig. 1a. The deflected shapes and section rotations of each segment are as follows.

For segment AC (i.e., for $0 \leqslant \bar{x} \leqslant a/L$)

$$\bar{Y}_1 = C_1\sin(\beta\bar{x}) + C_2\cos(\beta\bar{x}) + C_3\sinh(\alpha\bar{x}) + C_4\cosh(\alpha\bar{x}), \tag{33}$$

$$\Theta_1 = \lambda C_1\cos(\beta\bar{x}) - \lambda C_2\sin(\beta\bar{x}) + \delta C_3\cosh(\alpha\bar{x}) + \delta C_4\sinh(\alpha\bar{x}), \tag{34}$$

$$\bar{V}_1 = -\frac{b^2s^2}{\beta}C_1\cos(\beta\bar{x}) + \frac{b^2s^2}{\beta}C_2\sin(\beta\bar{x}) + \frac{b^2s^2}{\alpha}C_3\cosh(\alpha\bar{x}) + \frac{b^2s^2}{\alpha}C_4\sinh(\alpha\bar{x}), \tag{35}$$

$$\bar{M}_1 = -\lambda\beta C_1\sin(\beta\bar{x}) - \lambda\beta C_2\cos(\beta\bar{x}) + \delta\alpha C_3\sinh(\alpha\bar{x}) + \delta\alpha C_4\cosh(\alpha\bar{x}). \tag{36}$$

For segment CB (i.e., $a/L \leqslant \bar{x} \leqslant 1$):

$$\bar{Y}_2 = C_5\sin(\beta\bar{x}) + C_6\cos(\beta\bar{x}) + C_7\sinh(\alpha\bar{x}) + C_8\cosh(\alpha\bar{x}), \tag{37}$$

$$\Theta_2 = \lambda C_5 \cos(\beta\bar{x}) - \lambda C_6 \sin(\beta\bar{x}) + \delta C_7 \cosh(\alpha\bar{x}) + \delta C_8 \sinh(\alpha\bar{x}), \tag{38}$$

$$\bar{V}_2 = -\frac{b^2 s^2}{\beta} C_5 \cos(\beta\bar{x}) + \frac{b^2 s^2}{\beta} C_6 \sin(\beta\bar{x}) + \frac{b^2 s^2}{\alpha} C_7 \cosh(\alpha\bar{x}) + \frac{b^2 s^2}{\alpha} C_8 \sinh(\alpha\bar{x}), \tag{39}$$

$$\bar{M}_2 = -\lambda\beta C_5 \sin(\beta\bar{x}) - \lambda\beta C_6 \cos(\beta\bar{x}) + \delta\alpha C_7 \sinh(\alpha\bar{x}) + \delta\alpha C_8 \cosh(\alpha\bar{x}), \tag{40}$$

where Ω, ε, δ, and λ depend on the selected approach as described above. Eqs. (33)–(40) are given in terms of eight constants: (C_1–C_8) which must be determined from the following boundary and compatibility conditions. Boundary Conditions are

at $\bar{x} = 0$:

$$\bar{V}_1(0) + \bar{S}_a \bar{Y}_1(0) = 0, \tag{41a}$$

$$\bar{M}_1(0) - R_a \Theta_1(0) = 0 \tag{41b}$$

and at $\bar{x} = 1$:

$$\bar{V}_2(1) - \bar{S}_b \bar{Y}_2(1) = 0, \tag{41c}$$

$$\bar{M}_2(1) + R_b \Theta_2(1) = 0. \tag{41d}$$

Compatibility conditions are

at $\bar{x} = a/L$ (at the crack location):

$$\bar{Y}_1(a) = \bar{Y}_2(a) \text{ (deflection compatibility)}, \tag{41e}$$

$$\frac{\mathrm{d}\Theta_1(a)}{\mathrm{d}\bar{x}} = R_C[\Theta_2(a) - \Theta_1(a)] \text{ (spring equilibrium)}, \tag{41f}$$

$$\bar{V}_1(a) = \bar{V}_2(a) + \bar{S}_C \bar{Y}_1(a) \text{ (shear equilibrium)}, \tag{41g}$$

$$\frac{\mathrm{d}\Theta_1(a)}{\mathrm{d}\bar{x}} = \frac{\mathrm{d}\Theta_2(a)}{\mathrm{d}\bar{x}} \text{ (bending equilibrium)}. \tag{41h}$$

Using Eqs. (16)–(19) in the eight conditions described by Eqs. (41a)–(41h), the following homogeneous set of eight algebraic equations are obtained:

$$\begin{bmatrix} D_{11} & D_{12} & D_{13} & D_{14} & 0 & 0 & 0 & 0 \\ D_{21} & D_{22} & D_{23} & D_{24} & 0 & 0 & 0 & 0 \\ 0 & 0 & 0 & 0 & D_{35} & D_{36} & D_{37} & D_{38} \\ 0 & 0 & 0 & 0 & D_{45} & D_{46} & D_{47} & D_{48} \\ D_{51} & D_{52} & D_{53} & D_{54} & D_{55} & D_{56} & D_{57} & D_{58} \\ D_{61} & D_{62} & D_{63} & D_{64} & D_{65} & D_{66} & D_{67} & D_{68} \\ D_{71} & D_{72} & D_{73} & D_{74} & D_{75} & D_{76} & D_{77} & D_{78} \\ D_{81} & D_{82} & D_{83} & D_{84} & D_{85} & D_{86} & D_{87} & D_{88} \end{bmatrix} \begin{Bmatrix} C_1 \\ C_2 \\ C_3 \\ C_4 \\ C_5 \\ C_6 \\ C_7 \\ C_8 \end{Bmatrix} = 0, \tag{42}$$

where $D_{11} = -b^2 s^2/\beta$; $D_{12} = \bar{S}_a$; $D_{13} = b^2 s^2/\alpha$; $D_{14} = \bar{S}_a$; $D_{21} = -R_a\lambda$; $D_{22} = -\lambda\beta$; $D_{23} = -R_a\delta$; $D_{24} = \delta\alpha$; $D_{35} = -(b^2 s^2/\beta)\cos\beta - \bar{S}_b \sin\beta$; $D_{36} = (b^2 s^2/\beta)\sin\beta - \bar{S}_b \cos\beta$; $D_{37} = (b^2 s^2/\alpha)\cosh\alpha - \bar{S}_b \sinh\alpha$; $D_{38} = (b^2 s^2/\alpha)\sinh\alpha - \bar{S}_b \cosh\alpha$; $D_{45} = -\lambda\beta \sin\beta + R_b\lambda \cos\beta$; $D_{46} = -\lambda\beta \cos\beta - R_b\lambda \sin\beta$; $D_{47} = \delta\alpha \sinh\alpha + R_b\delta \cosh\alpha$; $D_{48} = \delta\alpha \cosh\alpha + R_b\delta \sinh\alpha$; $D_{51} = \sin(\beta a)$; $D_{52} = \cos(\beta a)$; $D_{53} = \sinh(\alpha a)$; $D_{54} = \cosh(\alpha a)$; $D_{55} = -\sin(\beta a)$; $D_{56} = -\cos(\beta a)$; $D_{57} = -\sinh(\alpha a)$; $D_{58} = -\cosh(\alpha a)$; $D_{61} = -\lambda\beta \sin(\beta a) + R_c\lambda \cos(\beta a)$; $D_{62} = -\lambda\beta \cos(\beta a) - R_c\lambda \sin(\beta a)$; $D_{63} = \delta\alpha \sinh(\alpha a) + R_c\delta \cosh(\alpha a)$; $D_{64} = \delta\alpha \cosh(\alpha a) + R_c\delta \sinh(\alpha a)$; $D_{65} = -R_c\lambda \cos(\beta a)$; $D_{66} = R_c\lambda \sin(\beta a)$; $D_{67} = -R_c\delta \cosh(\alpha a)$; $D_{68} = -R_c\delta \sinh(\alpha a)$; $D_{71} = -(b^2 s^2/\beta)\cos(\beta a) - \bar{S}_c \sin(\beta a)$; $D_{72} = (b^2 s^2/\beta)\sin(\beta a) - \bar{S}_c \cos(\beta a)$; $D_{73} = (b^2 s^2/\alpha)\cosh(\alpha a) - \bar{S}_c \sinh(\alpha a)$;

$D_{74} = (b^2 s^2/\alpha)\sinh(\alpha a) - \bar{S}_c \cosh(\alpha a)$; $D_{75} = (b^2 s^2/\beta)\cos(\beta a)$; $D_{76} = -(b^2 s^2/\beta)\sin(\beta a)$; $D_{77} = -(b^2 s^2/\alpha)\cosh(\alpha a)$; $D_{78} = -(b^2 s^2/\alpha)\sinh(\alpha a)$; $D_{81} = -\lambda\beta \sin(\beta a)$; $D_{82} = -\lambda\beta \cos(\beta a)$; $D_{83} = \delta\alpha \sinh(\alpha a)$; $D_{84} = \delta\alpha \cosh(\alpha a)$; $D_{85} = \lambda\beta \sin(\beta a)$; $D_{86} = \lambda\beta \cos(\beta a)$; $D_{87} = -\delta\alpha \sinh(\alpha a)$; and $D_{88} = -\delta\alpha \cosh(\alpha a)$.

Eq. (42) represents both the free-vibration and the stability eigenvalue problems of a Timoshenko beam-column with generalized end conditions and with a weakened section along the span. By making the determinant of the 8×8 matrix equal to zero, the undamped natural frequencies (ω) or the buckling loads (P_{cr}) of the member AB can be determined directly for a given value of the applied axial force or for a given frequency, and the corresponding modes of vibration or buckling modes from Eqs. (33)–(40) once the corresponding eigenvectors (C_1–C_8) are determined. The static buckling loads and modes are determined also from Eq. (42) by making $\omega = 0$ in the eigenvalue problem.

The five comprehensive examples that follow show the validity and simplicity of the proposed methods and Eqs. (33)–(42) using the two approaches described above. The first and second approach mentioned on each example refers to the effect of shearing forces induced by the axial load considering either the bending rotation only or the total slope, respectively. The objective of comparing both approaches is to assess the influence of the coupling effect of shear and axial force in the dynamic and stability behavior of Timoshenko beam-columns with a local flexibility at an arbitrary location. The first and second examples deal with the static stability (under tension and compression axial loads) of columns made of concrete and pultruded fiber reinforced polymer (PFRP), respectively. The results obtained are compared with different results from literature: Timoshenko and Gere [20], Wang et al. [17], the computational package SAP2000 [24], Aristizabal-Ochoa [13] and [25], and Roberts [26]. The third and fourth examples deal with the dynamic behavior of beams and beam-columns made of concrete and glass fiber reinforced polymer (GFRP), respectively. These two examples show the coupling effect between axial load and frequency as well as rotational inertia, shear deformations, and axial load. The results are compared with Aristizabal-Ochoa [27] and SAP2000 [24] according to different theories available in literature: Bernoulli–Euler, Rayleigh, Shear Beam, and Timoshenko. Finally, the fifth example compared the proposed model with experimental data available in the literature. All the examples are based on the assumption that the crack remains open, and in such a way nonlinearities due to the compressive stresses over a closing crack surface are avoided.

4. Proposed examples

4.1. Static stability of a partially restrained slender concrete column with a weakened section (step by step solution)

Using the left-side of the flowchart shown in Fig. 2 analyze a partially restrained square concrete column (500×500 mm) with a weakened section at $L/3$ from the bottom assuming the following properties: $E = 12\,\text{kN/mm}^2$; $G = 5\,\text{kN/mm}^2$; $A = 2.5 \times 10^5\,\text{mm}^2$; $A_s = 2.075 \times 10^5\,\text{mm}^2$; $I = 5.208 \times 10^9\,\text{mm}^4$; $\bar{m} = 0.600\,\text{kg/mm}$; $L = 6000\,\text{mm}$; $S_a = 15\,\text{kN/mm}$; $S_b = 25\,\text{kN/mm}$; $\kappa_a = 7.30 \times 10^7\,\text{kN-mm/rad}$; and $\kappa_b = 1.34 \times 10^7\,\text{kN-mm/rad}$. Determine: (I) the first three static compression buckling loads and corresponding shapes assuming that the magnitude of the flexural spring at the weakened section has a stiffness $\kappa_c = 1.04 \times 10^7\,\text{kN-mm/rad}$ and (II) the fundamental compression buckling load assuming that the column is pinned–pinned at both ends (i.e., $\kappa_a = \kappa_b = 0$, $S_a = S_b = \infty$). Compare the obtained results with those reported by Wang et al. [17].

Solution

(I) The static buckling loads are determined numerically using an iterative procedure (the Regula-falsi method is used herein) by making the determinant of Eq. (42) equal to zero and $\omega = 0$. An initial trial value of the critical load P is chosen and then the value of determinant is calculated. What follows are the steps necessary to carry out the stability analysis:

Step 1: Calculation of dimensionless parameters:

$$s = \sqrt{\frac{EI}{A_s G L^2}} = 0.0409, \quad R = \sqrt{\frac{I}{AL^2}} = 0.0241, \quad \bar{S}_a = \frac{S_a L}{A_s G} = 0.0867, \quad \bar{S}_b = \frac{S_b L}{A_s G} = 0.1446,$$

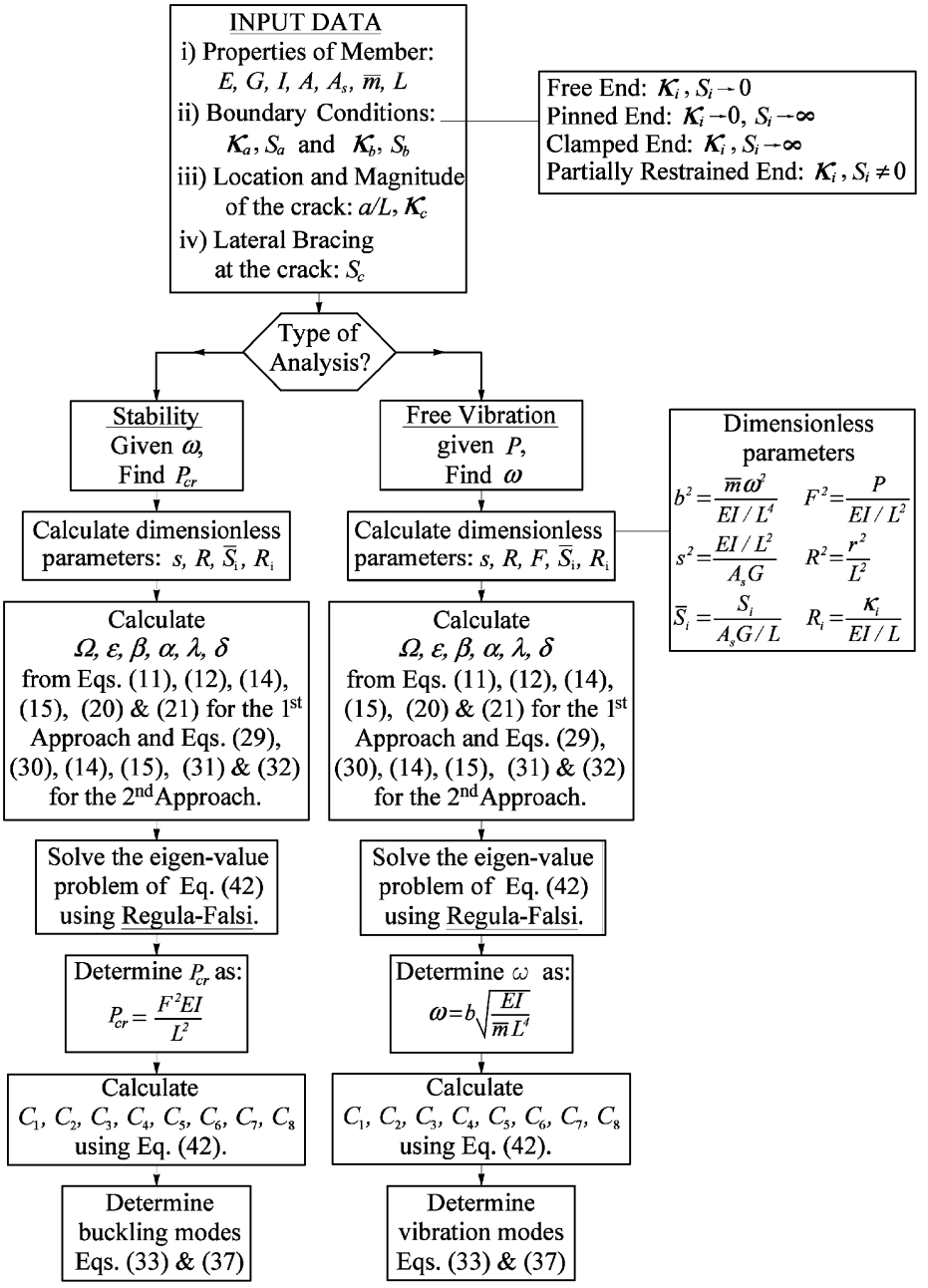

Fig. 2. Flowchart utilized in the stability and free vibration analyses.

Table 1
Example 1: steps 2 and 3

Buckling load	Ω Eq. (11)	ε ($\times 10^{-8}$) Eq. (12)	β Eq. (14)	α ($\times 10^{-5}$) Eq. (15)	λ Eq. (20)	δ ($\times 10^{-5}$) Eq. (21)	det ($\times 10^{-13}$) Eq. (42)	P_{cr} (kN)
1st mode	5.9427	−1.2685	3.4475	3.2669	3.3816	3.2669	−1.9900	20,238
2nd mode	13.8834	−1.2996	5.2694	2.1634	5.0450	2.1634	−6.6098	46,150
3rd mode	20.3251	−1.3238	6.3757	1.8046	5.9926	1.8046	−42.0067	66,328

Table 2
Example 1: step 4

Buckling load	C_1	C_2	C_3	C_4	C_5	C_6	C_7	C_8
1st mode	1	−1.18	−43,275.35	1.50	0.39	0.17	−43,275.35	1.50
2nd mode	1	0.08	−248,039.38	2.67	1.94	5.10	−248,039.38	2.67
3rd mode	1	2.96	−1,225,798.27	13.34	−1.38	−0.88	−1,225,798.27	13.34

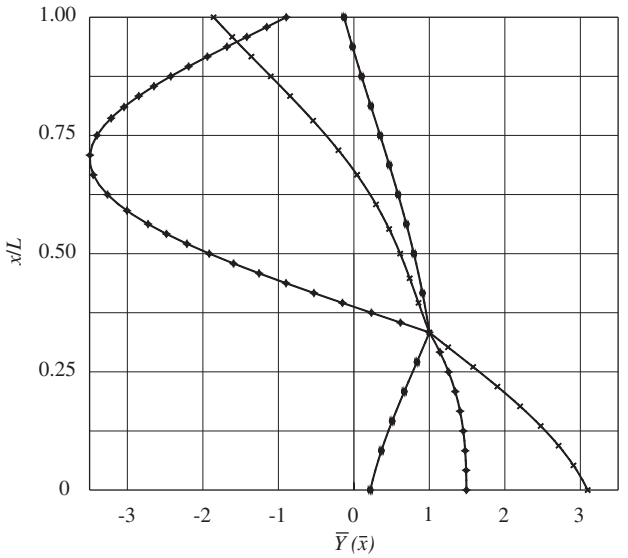

Fig. 3. Example 1: buckling shapes of a weakened beam-column at $x/L = 1/3$ calculated using 1st approach, 2nd approach, and SAP2000 [24]: (—●—) 1st mode, (—◆—) 2nd mode, and (—×—) 3rd mode.

Table 3
Example 1: critical loads, proposed method using both approaches and SAP2000 [24]

Mode	P_{cr} (kN)		
	Proposed method		SAP2000 [24]
	1st approach	2nd approach	
1	20,238	20,230	20,235
2	46,150	46,067	46,108
3	66,328	66,292	66,307

$$R_a = \frac{\kappa_a L}{EI} = 7.0084, \quad R_b = \frac{\kappa_b L}{EI} = 1.2865, \quad a/L = 1/3, \quad R_c = \frac{\kappa_c L}{EI} = 0.9985.$$

Step 2: Calculation of ω, ε, β, α, λ and δ corresponding to each buckling mode according to Eqs. (11), (12), (14), (15), (20) and (21) using the first approach (shear component proportional to the bending rotation) or according to Eqs. (29), (30), (14), (15), (31) and (32) using the second approach (shear component proportional to the total slope). Because of the low bending-to-shear ratio in this particular example, the results obtained using both approaches are practically identical to each other. Table 1 lists these values for the first three modes of buckling using the first approach.

Step 3: The process of making the determinant of Eq. (42) equal to zero is carried out numerically (iterative). The values of the determinant and the corresponding buckling loads P_{cr} for the first three

Table 4
Example 1: calculated results according to proposed model, Timoshenko and Gere [20], and Wang et al. [17]

R_c	P_{cr}/P^*								
	Proposed method			Timoshenko and Gere [20]			Wang et al. [17]		
	$S_c=0$	$S_c=8$	$S_c=16$	$S_c=0$	$S_c=8$	$S_c=16$	$S_c=0$	$S_c=8$	$S_c=16$
∞	1	2.57	4	1	2.5	4	1	NA	NA
1	0.3	2.25	4	NA	NA	NA	0.3	NA	NA
0	0	2	4	NA	NA	NA	0	NA	NA

Table 5
Example 2: beam-column properties

Column	EI ($\times 10^7$) (kN-mm^2)	GA_s ($\times 10^3$) (kN)	P^* (kN)	P^*/GA_s
$200\times200\times10$ mm, $L=4.50$ m, major axis [26]	78.50	5.34	382.60	0.07
$102\times51\times6.35$ mm, $L=0.40$ m, minor axis [26]	0.45	1.34	278.20	0.21
$152\times152\times6$ mm, $L=8.00$ m [30]	26.70	2.77	41.17	0.01
$152\times152\times6$ mm, $L=1.00$ m [30]	26.70	2.77	2635.18	0.95
$152\times152\times6$ mm, $L=0.40$ m [30]	26.70	2.77	16,469.90	5.95

modes are listed in the last two columns of Table 1. Notice that the values of the determinant are practically zero.

Step 4: Using again Eq. (42) the corresponding eigenvectors (i.e., values of C_1–C_8 for each buckling mode) are calculated. Table 2 lists these values for the first three modes of buckling.

Step 5: Using Eqs. (33) and (37) the shapes of each mode of buckling are determined. Fig. 3 shows these shapes calculated using both methods and using the SAP2000 program [24] modeling the column with 50 elements. Table 3 lists the critical loads corresponding to each buckling mode. The agreements in the buckling loads and mode shapes are excellent.

(II) To verify the proposed equations, the column was analyzed as simple supported at both ends (i.e., pinned–pinned column with $\kappa_a=\kappa_b=0$ and $S_a=S_b=\infty$) and with a weakened section at mid-height and the results were compared to those calculated by: (a) Timoshenko and Gere [20, pp. 72–73], and (b) Wang et al. [17]. These two models neglect the shear effects on the buckling load (i.e., Bernoulli–Euler model). When the bending-to-shear parameter s is dropped from Eq. (10) the same solutions are obtained regardless of the shear component approach under consideration. Table 4 lists the calculated results obtained by the proposed method and those by Timoshenko and Gere [20, pp. 72–73] and by Wang et al. [17] methods. The buckling loads are normalized with respect to $P^*(=\pi^2EI/L^2=17{,}133.63\,\text{kN})$ for three different values of lateral bracing ($S_cL/P^*=0$, 8 and 16) and for three different levels of cracking at mid-height ($R_c=0$, 1, and ∞).

The proposed method is more general than that by Wang et al. [17] since it includes the effects of: (1) the shear deformations along the span of each element; and (2) lateral bracing located at the cracked section. As expected, the lateral bracing at mid-height increased the buckling load by a factor of four in this particular example.

4.2. Static stability analyses under tension and compression of a series of columns made of pultruded fiber reinforced polymer

Using the left-side of the flowchart shown in Fig. 2 analyze five columns made of PFRP assuming the properties listed in Table 5. Determine: (I) the first three static buckling loads (tension and compression for

Table 6
Example 2: critical loads, pinned-pinned columns ($R_c = \infty$)

Column	Mode	P^+ (kN)[a]			P^-(kN)[b]
		1st approach (a)	2nd approach (b)	SAP2000 [24] (c)	1st approach (d)
$200 \times 200 \times 10$ mm, $L = 4.50$ m, major axis [26]	1	357.98	357.01	352.11	−5697.72
	2	1239.53	1189.48	1176.56	−6579.64
	3	2379.56	2093.45	2077.22	−7719.28
$102 \times 51 \times 6.35$ mm, $L = 0.40$ m, minor axis [26]	1	236.26	230.37	232.21	−1576.09
	2	721.78	607.93	611.67	−2061.87
	3	1279.52	872.85	877.09	−2619.41
$152 \times 152 \times 6$ mm, $L = 8.00$ m [30]	1	39.93	40.56	40.58	−2810.54
	2	155.47	155.45	155.65	−2925.62
	3	330.94	326.84	327.70	−3100.71
$152 \times 152 \times 6$ mm, $L = 1.00$ m [30]	1	1649.58	1350.45	1351.37	−4419.85
	2	4188.28	2193.55	2195.95	−6957.94
	3	6833.25	2480.31	2483.36	−9603.74
$152 \times 152 \times 6$ mm, $L = 0.40$ m [30]	1	5506.64	2371.19	2371.65	−8276.60
	2	12,181.11	2658.23	2658.79	−14,951.13
	3	18,915.38	2719.19	2719.77	−21,685.32

[a] P^+ denotes compression axial load.
[b] P^- denotes tension axial load.

Table 7
Example 2: critical loads, pinned–pinned columns ($R_c = 1$)

Column	Mode	P^+ (kN)[a]					P^-(kN)[b]
		$(P^*/A_sG) \neq 0$ 1st approach (a)	$(P^*/A_sG) \neq 0$ 2nd approach (b)	$(P^*/A_sG) = 0$ (c)	Wang et al. [17] (d)	SAP2000 [24] (e)	1st Approach (f)
$200 \times 200 \times 10$ mm, $L = 4.50$ m, major axis [26]	1	145.78	145.68	149.75	149.77	145.03	−5485.79
	2	698.09	687.69	789.19	789.35	680.25	−6038.09
	3	2038.00	1843.64	2813.76	2815.80	1828.25	−7378.00
$102 \times 51 \times 6.35$ mm, $L = 0.40$ m, minor axis [26]	1	101.25	100.71	108.90	108.89	103.3	−1441.25
	2	433.64	401.84	573.84	573.96	445	−1773.63
	3	1116.76	809.92	2045.96	2047.45	998.19	−2456.76
$152 \times 152 \times 6$ mm, $L = 8.00$ m [30]	1	16.02	16.01	16.11	16.12	16.02	−2786.02
	2	82.49	82.42	84.93	84.95	82.45	−2852.49
	3	275.61	273.14	302.81	303.04	273.55	−3045.60
$152 \times 152 \times 6$ mm, $L = 1.00$ m [30]	1	800.29	751.62	1031.10	1031.50	751.65	−3570.29
	2	2735.42	1835.04	5425.67	5436.70	1835.61	−5505.42
	3	6074.21	2423.81	19,255.20	19,394.06	2424.92	−8844.21
$152 \times 152 \times 6$ mm, $L = 0.40$ m [30]	1	3062.04	1937.52	6446.65	6446.90	1937.66	−5832.04
	2	8415.05	2561.21	33,972.43	33,979.35	2561.91	−11,185.05
	3	16,991.01	2708.11	121,124.96	121,212.89	2709.00	−19,761.01

[a] P^+ denotes compression axial load.
[b] P^- denotes tension axial load.

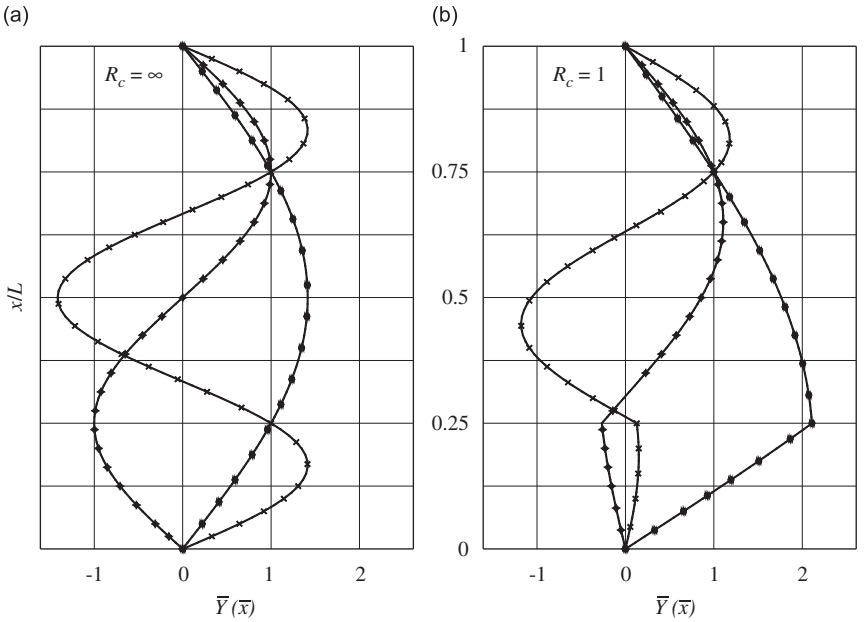

Fig. 4. Example 2: buckling shapes of a pinned–pinned beam-column under tension and compression calculated using 1st approach (P^+ and P^-), 2nd approach (P^+), and SAP2000 [24] (P^+): (a) $R_c = \infty$; (b) $R_c = 1$: (—●—) 1st mode, (—◆—) 2nd mode, and (—×—) 3rd mode.

$\omega = 0$) and mode shapes of a pinned–pinned column assuming that $R_c = \infty$ and 1 at $x/L = 0.25$ from the bottom end. Compare the results obtained using both approaches with those presented by Roberts [26], Wang et al. [17], Aristizabal-Ochoa [13] and [25], and also with those using SAP2000 computer program [24] (modeled with 50 segments along the column height L); and (II) the first three buckling loads and modes (under tension and compression) for a clamped–pinned column whose properties are listed in Table 5 (row 5) assuming that $R_c = \infty$ and 1 at $x/L = 0.25$ from the fixed end.

Solution:

(I) In Table 5 are the values of EI, GA_s, Euler load ($P^* = \pi^2 EI/L^2$) and the ratio P^*/GA_s for each of the columns under analysis. Tables 6 and 7 show the results of the first three buckling loads (tension and compression) obtained using both approaches, and those using the SAP2000 program [24] (modeled with 50 segments along the column height L) for $R_c = \infty$ and 1 at $x/L = 0.25$, respectively. Fig. 4 shows the corresponding buckling modes. Based on the results shown in Fig. 4 and those listed in Tables 6 and 7, the following conclusions can be drawn:

(1) The compressive and tensile critical loads listed in Table 6 [columns (a) and (d)] obtained with the first approach of the proposed model for the case of $R_c = \infty$ (uncracked column) are practically identical to those calculated using the expression: $P_{cr} = P_E/(1 + P_{cr}/GA_s)$ which yields the following quadratic expression: $P_{cr}^2 + GA_sP_{cr} - GA_sP_E = 0$ whose solution for a pinned–pinned column is: $P_{cr} = (GA_s/2)\left(\pm\sqrt{1 + (4P_E/GA_s)} - 1\right)$. This equation is referred as Haringx's formula and detailed by Bazant [28] for the compression buckling load and most recently presented by Aristizabal-Ochoa [25] for both compression and tension loads, as shown above. Notice that the 1st mode compressive critical loads listed in Table 6 [column (a)] are also those reported by Roberts [26]. The compressive critical loads listed in Table 6 [columns (b) and (c)] obtained using the second approach and the SAP2000 program [24] (modeled with 50 segments along the column) are similar to those obtained using the first approach if the column is very slender (see case of $152 \times 152 \times 6$ mm, $L = 8000$ mm). On the other hand, the results are quite different (lower buckling loads) using the second approach and SAP2000 [24] [see columns (b) and (c), Table 6] from those using the first approach especially when the

Table 8
Example 2: critical loads, clamped-pinned columns ($R_c = \infty$ and 1)

Column	Mode	$R_c = \infty$				$R_c = 1$			
		P^+ (kN)[a] 1st approach	P^+ (kN)[a] 2nd approach	P^+ (kN)[a] SAP2000 [24]	P^- (kN)[b] 1st approach	P^+ (kN)[a] 1st approach	P^+ (kN)[a] 2nd approach	P^+ (kN)[a] SAP2000 [24]	P^- (kN)[b] 1st approach
$152 \times 152 \times 6$ mm, $L = 0.40$ m	1	7268.12	2445.13	2445.75	−6089.36	6985.11	2309.40	2309.56	−4102.07
	2	14,049.21	2666.00	2666.83	−12,895.27	9003.84	2564.38	2565.05	−11,053.71
	3	20,813.46	2720.92	2721.80	−19,664.05	17,025.93	2708.17	2709.04	−19,589.87

[a] P^+ denotes compression axial load.
[b] P^- denotes tension axial load.

column is short. This discrepancy is due to the fact that the second approach and the SAP2000 [24] program include the effects of shear deformations using a much more conservative approach. These results confirm that the first approach is more accurate whereas the second approach yields more conservative buckling loads [20, p. 135]. These features are further discussed by Aristizabal-Ochoa [13] and also shown by the results of the weakened Timoshenko beam-column analyzed herein.

(2) The compressive and tensile critical loads obtained with the proposed method for the case of $R_c = 1$ and including the shear effects are listed in Table 7 [columns (a), (b) and (f)]. Also in columns (c) and (d) are listed the compressive critical loads for the case of $R_c = 1$ but neglecting shear effects (Bernoulli–Euler column) obtained using the proposed method and that by Wang et al. [17]. The results are practically identical to each other. Again, those calculated using the second approach and the SAP2000 program [24] are similar to those obtained using the first approach for the slender column (see case of $152 \times 152 \times 6$ mm, $L = 8000$ mm). However, the results are quite different (lower) from those using the proposed method when the column is short.

(3) The buckling load capacities in tension and compression are reduced substantially by the shear effects, particularly in short columns. For example, column $152 \times 152 \times 6$ mm with $L = 0.40$ m and $R_c = 1$ at $x/L = 0.25$, its 1st mode compressive critical load, calculated using the first approach, is reduced from 6447 to 3062 kN and its tensile critical load is also reduced from infinity to 5832 kN when the shear effects are included. Therefore, it is very important to include the shear effects in short columns.

(4) Fig. 4 shows that the buckling modes of all five cases studied of a column pinned–pinned are not influenced by the shear effects and the selected approach in both cases of $R_c = \infty$ and 1. The effect of a crack at $x/L = 0.25$ is that of a slope discontinuity at the crack. Similar to Fig. 3, the buckling modes [determined using Eqs. (33) and (37)] using both approaches and to those obtained using the SAP2000 program [24] are in perfect agreement.

(II) In Table 8 are the buckling loads (compression and tension for $R_c = \infty$ and 1) and Figs. 5 and 6 show the corresponding buckling shapes of the first three modes for the clamped–pinned column according to the proposed method. The compression buckling loads and modes according to the SAP2000 program [24] are also included for comparison. This program and the second approach do not have the capability of determining the tension buckling modes since they do not include the effects of the shear force component of the applied axial force according to the "modified" approach (using the bending rotation) as proposed by Timoshenko and Gere [20]. This has been discussed recently by Aristizabal-Ochoa [13,25] on the stability of elastomeric bearings under tension presented by Kelly [29].

Figs. 5 and 6 show clearly that for clamped–pinned columns, the buckling modes in compression and tension are quite different from each other and are highly sensitive to the shear effects just mentioned. In addition, the values of the compression buckling loads calculated using the first approach are also quite different to those obtained using the second approach and the SAP2000 program [24]. These differences in the modal shapes of Fig. 5 were not observed in the case of the pinned–pinned column (Fig. 4) and that of the

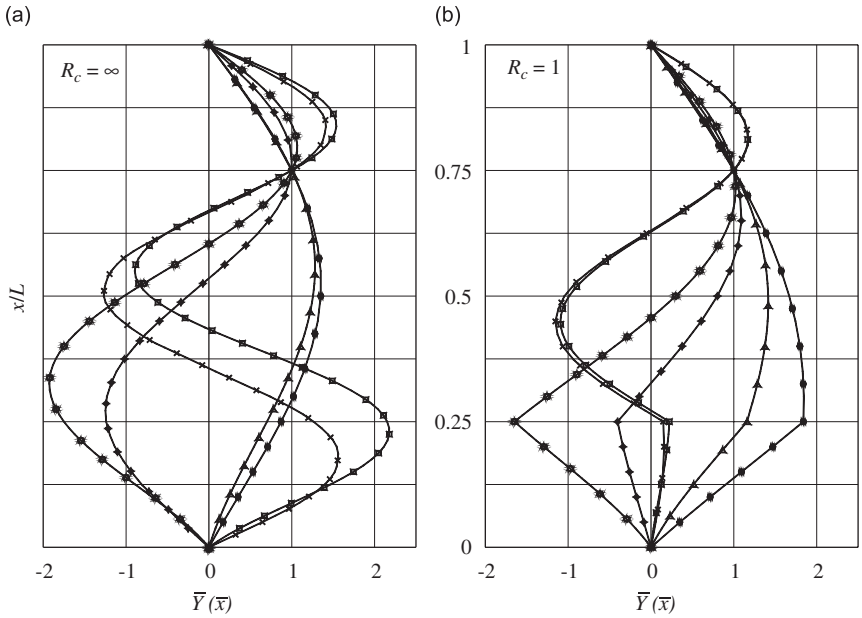

Fig. 5. Example 2: buckling shapes of a clamped–pinned beam-column under compression: (a) $R_c = \infty$; and (b) $R_c = 1$: (—△—) 1st mode, 1st approach; (—⊖—) 2nd mode, 1st approach; (—⊟—) 3rd mode, 1st approach; (—●—) 1st mode, 2nd approach and SAP2000 [24]; (—◆—) 2nd mode, 2nd approach and SAP2000 [24]; and (—×—) 3rd mode, 2nd approach and SAP2000 [24].

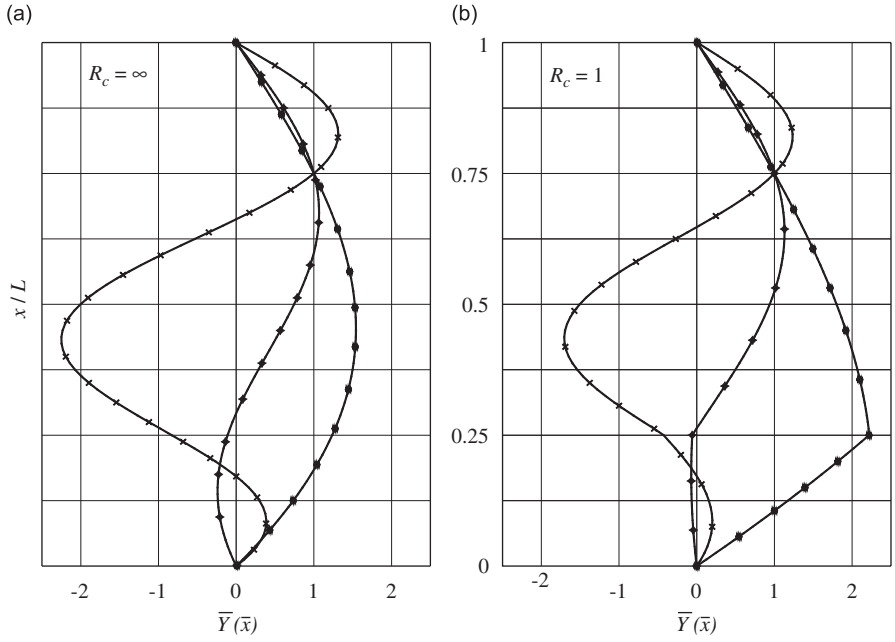

Fig. 6. Example 2: buckling shapes of a clamped–pinned FRP column under tension (1st approach): (a) $R_c = \infty$; and (b) $R_c = 1$: (—●—) 1st mode, (—◆—) 2nd mode, and (—×—) 3rd mode.

slender concrete column of Example 1 (Fig. 3). However, the compressive buckling loads listed in Tables 6–8 indicate that the values obtained using the second approach and the SAP2000 program [24] are quite different from those calculated with the first approach, except for the slender columns (i.e., those with a total height over 4.50 m whose behavior is controlled by bending rather than shear).

Table 9
Example 3: steps 2 and 3 ($P = 0$)

Mode of vibration	Ω Eq. (11)	ε Eq. (12)	β Eq. (14)	α Eq. (15)	λ Eq. (20)	δ Eq. (21)	Frequency (Hz)
1st	0.0746	−66.2763	2.8663	2.8402	2.8277	2.8792	11.62
2nd	0.3686	−327.2690	4.2968	4.2102	4.1694	4.3403	25.82
3rd	1.1795	−1046.4937	5.7923	5.5849	5.4897	5.8988	46.18

Table 10
Example 3: step 4 ($P = 0$)

Mode of vibration	C_1	C_2	C_3	C_4	C_5	C_6	C_7	C_8
1st	1	−0.07	−0.63	0.80	0.78	0.24	−1.20	1.22
2nd	1	1.88	−1.22	1.42	0.85	2.95	−3.50	3.43
3rd	1	−16.26	7.03	−5.70	4.26	−7.61	−22.34	22.29

4.3. Dynamics of a partially restrained square concrete column with a weakened section (step by step solution)

Using the right-hand side of the flowchart shown in Fig. 2 determine the variation of the natural frequencies corresponding to the first three modes of vibration with the applied axial load P for the partially restrained square concrete column (500×500 mm) of Example 1 assuming that has a weakened section at $x = L/3$ with $\kappa_c = 1.04 \times 10^7$ kN-mm/rad. Analyze the column using both approaches.

Solution:

To determine the effects of the applied axial load on the natural frequencies and modal shapes the determinant of Eq. (42) must be made equal to zero for different values of P. The natural frequencies must be determined numerically using an iterative procedure (the Regula-falsi method is used herein) to carry out such analysis. An initial trial value of the natural frequency is chosen and then the value of determinant is calculated. What follows are the steps necessary to carry out the dynamic analysis.

Step 1: Calculation of dimensionless parameters: R, $\bar{S}_a$, $\bar{S}_b$, R_a, R_b, a/L and R_c. These are identical to those in Example 1. However, the parameter F corresponding to the applied axial load is varied from the critical load in compression (resulting in $\omega = 0$) to some value of P in tension (chosen arbitrarily as $P = -10{,}000$ kN for this example).

Step 2: Calculation of ω, ε, β, α, λ and δ corresponding to each mode of vibration according to Eqs. (11), (12), (14), (15), (20) and (21) using the first approach or Eqs. (29), (30), (14), (15), (31) and (32) using the second approach. These values are listed in the first six columns of Table 9 for the particular case of $P = 0$. As in Example 1, the results obtained using both approaches are practically identical to each other, because of the low bending-to-shear ratio.

Step 3: The process of making the determinant of Eq. (42) equal to zero is carried out numerically (iterative). The values of frequency in Hz ($f = \omega/2\pi$) are listed in the last column of Table 9.

Step 4: Using again Eq. (42) the corresponding eigenvectors (i.e., values of C_1–C_8 for each mode of vibration) are calculated. Table 10 lists these values for the first three modes of buckling for the particular case of $P = 0$.

Step 5: Each mode of vibration is determined using Eqs. (33) and (37). Fig. 7 shows the modal shapes calculated using Eqs. (33) and (37) by both approaches and also the modal shapes obtained using the SAP2000 program [24] for the particular case $P = 0$. The modal shapes using the three methods are in excellent agreement with each other.

Fig. 8 shows the variation of the natural frequency with the applied axial load (tension and compression) using the first approach. Table 11 lists the values of the frequencies obtained using both approaches and

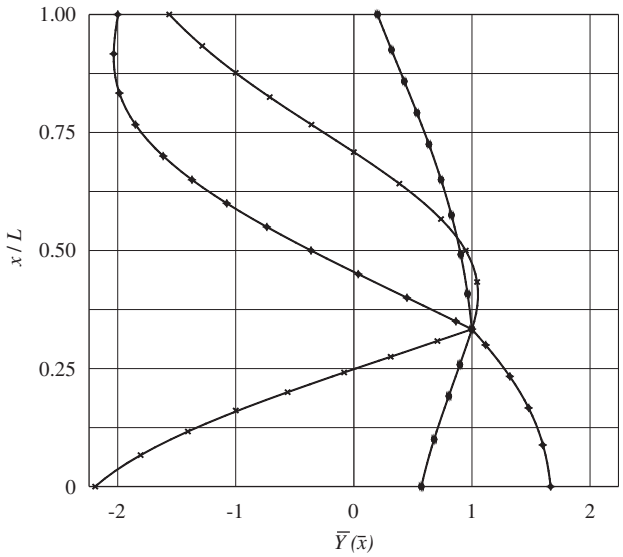

Fig. 7. Example 3: vibration shapes of a weakened column calculated using 1st approach, 2nd approach, and SAP2000 [24]: (—●—) 1st mode, (—◆—) 2nd mode, and (—×—) 3rd mode.

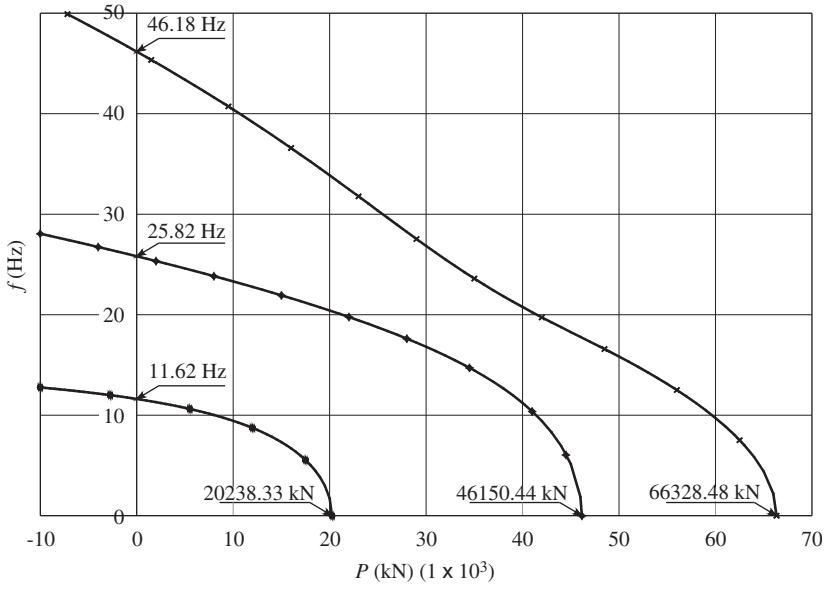

Fig. 8. Example 3: variation of natural frequencies with applied axial load for a weakened column: (—●—) 1st mode, (—◆—) 2nd mode, and (—×—) 3rd mode.

a model of the column with 50 elements using the SAP2000 program [24] for $P = 0$, showing that for this particular case the results from both approaches and the FEM model are within 1.1%.

It is important to emphasize that the first approach [i.e., that based on Eqs. (3)–(21) that assumes that the shear component induced by the applied axial load is proportional to the bending rotation] is the only one capable to capture buckling under tension. The second approach and the SAP2000 program which uses the Bernoulli–Euler beam do not capture the phenomenon of buckling under tension.

Table 11
Example 3: natural frequencies (Hz), proposed method using both approaches and SAP2000 [24]

Mode	Frequency (Hz) ($P = 0$)		
	Proposed method		SAP2000 [24]
	1st approach	2nd approach	
1	11.62	11.62	11.62
2	25.82	25.82	25.89
3	46.18	46.18	46.69

Table 12
Example 4: natural frequencies (Hz) of a pinned-free member

Beam length, L (m)	Mode	$R_c = \infty$					$R_c = 1$
		Flexural beam (a)	PM[a] $s = 0$ and $R \neq 0$ (b)	PM[a] $s \neq 0$ and $R \neq 0$ (c)	PM[a] $s = \infty$ and $R \neq 0$ (d)	Shear-beam [27] (e)	PM[a] $s \neq 0$ and $R \neq 0$ (f)
4.00	1	0.0304	0.0303	0.0293	0.1141	0.1141	0.0169
	2	0.0985	0.0974	0.0873	0.1962	0.1962	0.0829
	3	0.2056	0.2012	0.1630	0.2770	0.2770	0.1423
1.00	1	0.4865	0.4610	0.3284	0.4546	0.4546	0.2281
	2	1.5765	1.3843	0.6882	0.7808	0.7808	0.6579
	3	3.2893	2.6332	1.0284	1.0993	1.0993	1.0133
0.40	1	3.0406	2.3223	1.0176	1.0903	1.0904	0.8844
	2	9.8533	5.8721	1.5704	1.5819	1.5819	1.5704
	3	20.5582	9.8350	2.0041	2.0414	2.0414	1.9112

[a]PM denotes proposed model.

4.4. Effects of rotational inertia, shear deformations, and axial load on the free vibration of a weakened pinned-free GFRP beam

Using the first approach and assuming the following properties for a pinned-free beam: $E = 24.05932\,\text{kN/mm}^2$; $G = 3.03728\,\text{kN/mm}^2$; $A = 2664\,\text{mm}^2$; $A_s = 912\,\text{mm}^2$; $I = 11{,}097{,}568\,\text{mm}^4$; and $\bar{m} = 0.0067932\,\text{kg/mm}$, cracked at mid-span with $R_c = 1$; determine: (I) the natural frequencies corresponding to the first three modes of vibration for three different span lengths ($L = 4.0$, 1.0 and 0.4 m). Compare the obtained results for the uncracked beam (i.e., $R_c = \infty$) using the proposed model (including the simultaneous effects of flexural and shear deformations, translational and rotational inertias) with those modeled as a flexural member (Bernoulli–Euler), and as a shear beam (as suggested by Aristizabal-Ochoa [27] including the effects of the beam rotational inertia); (II) the modal shapes corresponding to the first three-modes of vibration for two different span lengths ($L = 4.0$ and 0.4 m) for the uncracked beam; and (III) the variation of the first three natural frequencies with the applied axial load (tension and compression) for the uncracked beam with $R_c = 1$ at mid-span.

Solution:

(I) Table 12 lists the natural frequencies corresponding to the first three modes of vibration for the three span lengths under consideration with the member modeled as a flexural member (Bernoulli–Euler theory), using the proposed model (including the simultaneous effects of flexural and shear deformations, translational and rotational inertias), and as a shear beam (as suggested by Aristizabal-Ochoa [27] including rotational inertia). The values listed in columns (b)–(d) are according to the proposed method as

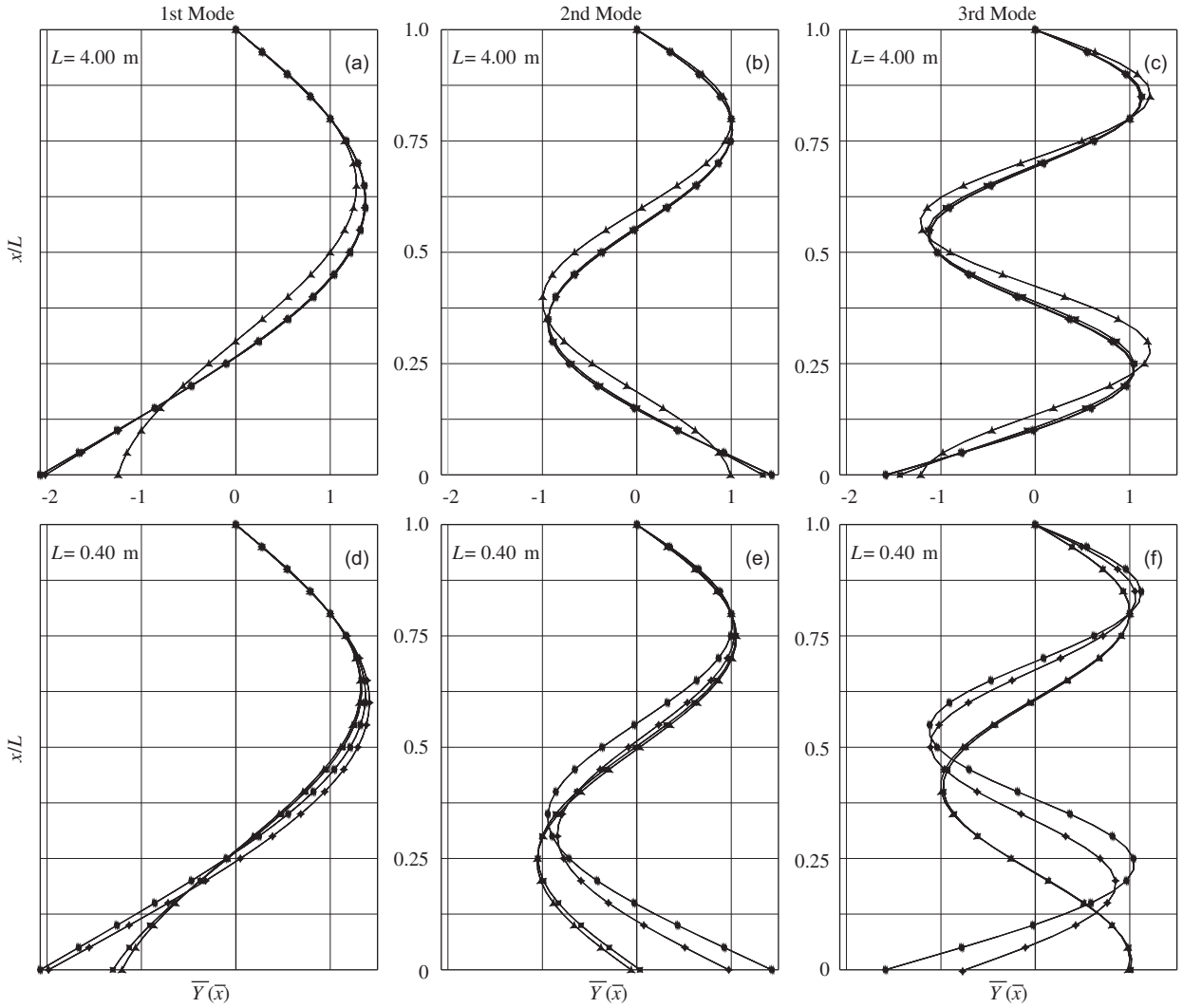

Fig. 9. Example 4: vibration shapes of a pinned-free GFRP beam: (a) 1st mode, $L = 4.00$ m; (b) 2nd mode, $L = 4.00$ m; (c) 3rd mode, $L = 4.00$ m; (d) 1st mode, $L = 0.40$ m; (e) 2nd mode, $L = 0.40$ m; and (f) 3rd mode, $L = 0.40$ m: (—■—) Timoshenko, (—●—) Bernoulli, (—◆—) Rayleigh, and (—▲—) shear building [27].

indicated: (1) $s = 0$ and $R \neq 0$, [i.e., neglecting shear deformations but including rotational inertia (Rayleigh theory)]; (2) $s \neq 0$ and $R \neq 0$ [i.e., including shear deformations and rotational inertia (Timoshenko theory)]; and (3) $s = \infty$ and $R \neq 0$ [i.e., neglecting flexural deformations but including rotational inertia (shear-beam theory)]. Column (f) lists the values according to the proposed method with $s \neq 0$ and $R \neq 0$ (Timoshenko theory) and $R_a = 1$ at mid-span. Based on the results listed in Table 12, the following conclusions can be drawn:

(i) The values listed in columns (a) and (b) are very similar to each other for the slender beam ($L = 4.00$ m) only. For shorter members ($L = 1.0$ and 0.4 m), the results listed in column (a) which are based on the classic Bernoulli–Euler theory are different from those listed in column (b) which are based on Rayleigh theory and quite different from those listed in column (c) which are based on Timoshenko theory. These differences become even larger in the higher modes of vibration in which the effects of rotational inertia and shear deformations become significant. These effects are discussed by Aristizabal-Ochoa [19].

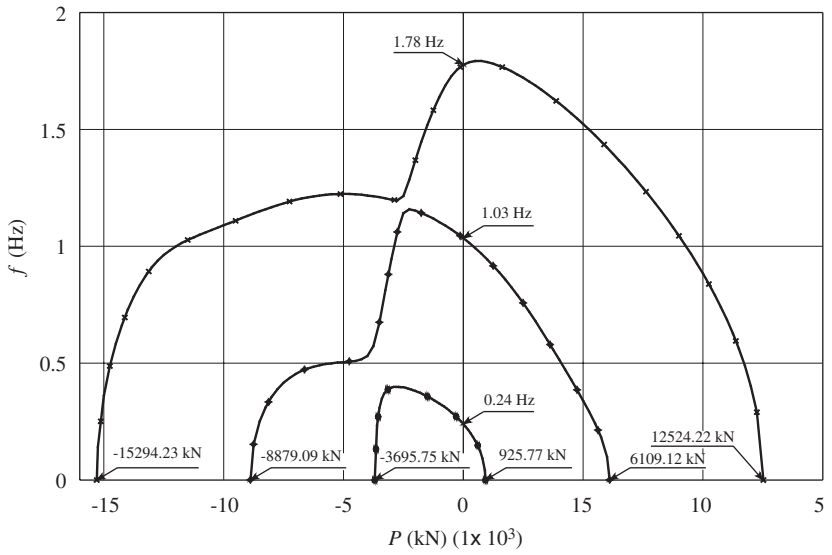

Fig. 10. Example 4: variation of the first three natural frequencies with the applied axial load for a pinned-free column ($L = 0.40$ m) weakened at mid-span: (—●—) 1st mode; (—◆—) 2nd mode; and (—×—) 3rd mode.

(ii) The values listed in column (d) are identical to those of column (e) calculated using the formula presented by Aristizabal-Ochoa [27] for shear beams with the rotational inertia effects included.

(iii) As expected, a flexural crack along the member and away from its ends, reduce significantly its natural frequencies, particularly the 1st mode frequency in slender members, as indicated by the values listed in column (f).

(iv) Fig. 9a–f show the modal shapes corresponding to the first three modes of vibration for two different span lengths ($L = 4.0$ and 0.4 m, respectively) calculated using Bernoulli–Euler, Rayleigh, Shear Beam, and Timoshenko (i.e., the proposed model) theories. Fig. 9a–c show that the first three modes of vibration calculated using Bernoulli–Euler, Rayleigh and Timoshenko theories are very similar to each other for the slender beam ($L = 4.0$ m) only. In slender members the dynamic behavior is controlled by flexural deformations and translational inertia and the effects of shear deformations and rotatory inertia are not significant, particularly in the lower modes of vibration. For the short member ($L = 0.40$ m), however, the frequencies and modal shapes (Fig. 9d–f) are controlled by shear deformations and rotatory inertia, this is why the results obtained using the models of Timoshenko and that of the shear beam are practically identical to each other. These effects were also discussed by Aristizabal-Ochoa [19].

(II) Fig. 10 shows the variation of the first three natural frequencies with the applied axial load (tension and compression) for a hinged-free beam of $L = 400$ mm with a weakened section at mid-span ($R_c = 1$). The values indicated along the vertical axis are the natural frequencies when the axial load is zero. The values indicated along the horizontal axis are the static buckling loads in tension (negative) and compression (positive). In general, compression loads reduce the natural frequencies. Tension loads increase the natural frequencies up to some peak values, and then they are reduced dramatically. In this particular example, at a tension load of $P = 2850$ kN the 1st mode natural frequency becomes a maximum ($f = 0.3984$ Hz), and at a tension load of $P = 3696$ kN the member reaches tension buckling and the 1st mode natural frequency is reduced to zero.

4.5. *Simply supported aluminum rectangular beam (experimental comparison)*

In order to compare the proposed model with more results available in literature, the particular case of a simply supported aluminum beam, tested by Chondros et al. [4] and Chondros [5] in the University of Patras, Greece, is studied using the first approach and compared with the experimental results. The properties of the

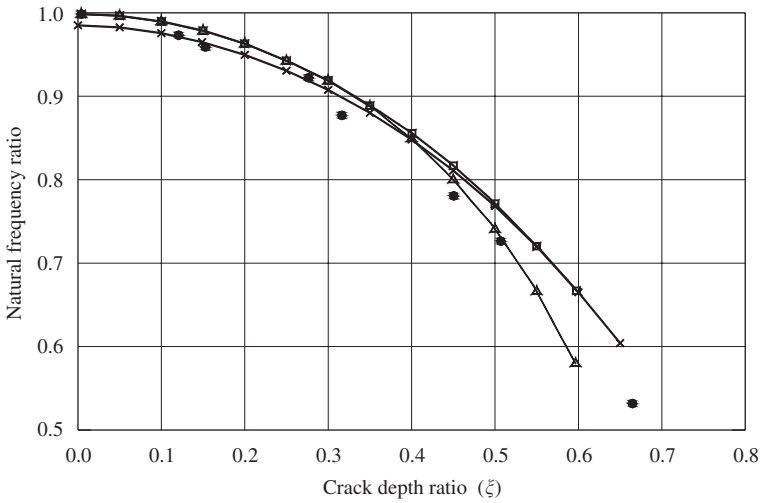

Fig. 11. Example 5: variation of the natural frequency ratio with the crack depth ratio for a simply supported beam: (—×—) proposed model; (—□—) local flexibility [4,5]; (—△—) continuous crack [4,5]; and (●) experimental results [4,5].

member are as follows: $E = 72\,\mathrm{kN/mm^2}$; $G = 26.67\,\mathrm{kN/mm^2}$; $A = 152.4\,\mathrm{mm^2}$ (rectangular section: $6 \times 25.4\,\mathrm{mm}$); $A_s = 126.5\,\mathrm{mm^2}$; $I = 8193.5\,\mathrm{mm^4}$; $\bar{m} = 4.267 \times 10^{-4}\,\mathrm{kg/mm}$; and $L = 235\,\mathrm{mm}$.

The flexibility induced by the crack was calculated according to Chondros [5] following the fracture mechanics formulation (for a rectangular section assuming open crack):

$$\kappa_c = \frac{EI}{6\pi h(1-\nu^2)\Phi_I(\xi)}, \tag{43}$$

where $\Phi_I(\xi)$ is defined as

$$\Phi_I(\xi) = 0.6272\xi^2 - 1.04533\xi^3 + 4.5948\xi^4 - 9.9736\xi^5 + 20.2948\xi^6 - 33.0351\xi^7 + 47.1063\xi^8 - 40.7556\xi^9 + 19.6\xi^{10}. \tag{44}$$

The variable ξ into Eq. (44) is the ratio of the crack depth to the height of the rectangular cross section.

Note that the results presented in Fig. 11 agree well with those reported by Chondros et al. [4] and Chondros [5] assuming local flexibility and with those obtained from the experimental test performed on the aluminum beam.

5. Summary and conclusions

The stability and free vibration analyses of a Timoshenko beam-column with generalized end conditions (i.e., with semi-rigid connections and lateral bracings at both ends) and weakened by a cracked section along its span are presented. The magnitude and location of the weakened section are both arbitrary and independent of each other. The magnitude of the crack is modeled as an intermediate flexural connection of zero length producing a member with two-segments with rotational discontinuity at the crack location but of identical lateral deflection. It is shown that the buckling loads in tension and compression are reduced substantially by the shear effects, particularly in short beam-columns. As expected, the lateral bracing located at the weakened section alleviates the detrimental effects of the crack. Therefore, it is very important to include these effects. The proposed model and equations are general including the following effects: (1) the coupling between the shear and bending deformations along the member's span; (2) the coupling between the translational and rotational masses of the member uniformly distributed along its span; (3) static axial loads (tension or compression) applied at the ends; and (4) shear forces along the member induced by the applied

axial loads as the beam-column deforms according to two different approaches proposed by Timoshenko and Gere [20].

The effects of shear deformations on the stability and natural frequencies of slender beam-columns can be neglected and models based on the Bernoulli–Euler theory give acceptable results. However, for intermediate and short span members these effects must be included since they reduced their buckling loads and natural frequencies. It was found that the method based on Eqs. (3)–(21) (denoted as the first approach in this paper that assumes that the shear component induced by the applied axial load is proportional to the bending rotation) is more accurate and the only one capable to capture the phenomenon of buckling under tension in members with low shear stiffness. The second approach presented herein (that assumes that the shear component induced by the applied axial load is proportional to the total slope of the member axis) and the SAP2000 [24] which uses the Bernoulli–Euler beam do not capture the phenomenon of buckling under tension. Finally, results obtained from the stability and natural vibration analyses of short beam-columns using the first approach differ greatly from those obtained using the second approach and the SAP2000 program [24]. For this reason, the first approach which is identical to the "modified" method (Haringx column) proposed by Timoshenko and Gere is strongly recommended in the stability and free vibration analyses of structures made of beam-columns.

Acknowledgments

The research presented in this paper was carried out at the National University of Colombia, School of Mines at Medellín, while the first two authors were members of the Structural Stability Research Group (GES). The authors wish to acknowledge the National University of Colombia (DIME) for providing financial support and to Professor Gabriel Gomez (Department of Civil Engineering, National University of Colombia) for his encouragement.

References

[1] N. Anifantis, A. Dimarogonas, Stability of columns with a single crack subjected to follower force and vertical loads, *International Journal of Solids and Structures* 19 (1983) 281–291.
[2] F.Y. Cheng, C.P. Pantelides, Dynamic Timoshenko beam-columns on elastic media, *Journal of Structural Engineering-ASCE* 114 (7) (1988) 1524–1550.
[3] A.D. Dimarogonas, Vibration of cracked structures: a state of the art review, *Engineering Fracture Mechanics* 55 (1996) 831–857.
[4] T.G. Chondros, A.D. Dimarogonas, J. Yao, A continuous cracked beam vibration theory, *Journal of Sound and Vibration* 215 (1) (1998) 17–34.
[5] T.G. Chondros, The continuous crack flexibility model for crack identification, *Fatigue and Fracture of Engineering Materials and Structures* 24 (2001) 643–650.
[6] I. Takahashi, Vibration and stability of non-uniform cracked Timoshenko beam subjected to follower force, *Computers and Structures* 71 (1999) 585–591.
[7] S.D. Panteliou, T.G. Chondros, V.C. Argyrakis, A.D. Dimarogonas, Damping factor as an indicator of crack severity, *Journal of Sound and Vibration* 241 (2) (2001) 235–245.
[8] E.I. Shifrin, R. Ruotolo, Natural frequencies of a beam with an arbitrary number of cracks, *Journal of Sound and Vibration* 222 (3) (1999) 409–423.
[9] Q.S. Li, Buckling of multi-step cracked columns with shear deformation, *Engineering Structures* 23 (2001) 356–364.
[10] Q.S. Li, Vibratory characteristics of Timoshenko beams with arbitrary number of crack, *Journal of Engineering Mechanics-ASCE* (11) (2003) 1355–1359.
[11] Q.S. Li, Classes of exact solutions for buckling of multi-step non-uniform columns with an arbitrary number of cracks subjected to concentrated and distributed axial loads, *International Journal of Engineering Science* 41 (2003) 569–586.
[12] C.M. Wang, K.H. Ng, S. Kitipornchai, Stability criteria for Timoshenko columns with intermediate and end concentrated axial loads, *Journal of Constructional Steel Research* 58 (9) (2002) 1177–1193.
[13] J.D. Aristizabal-Ochoa, Column stability and minimum lateral bracing: effects of shear deformations, *Journal of Engineering Mechanics-ASCE* 130 (10) (2004) 1223–1232.
[14] Y.Y. Lee, C.M. Wang, S. Kitipornchai, Vibration of Timoshenko beams with internal hinge, *Journal of Engineering Mechanics-ASCE* 129 (3) (2003) 293–301.
[15] S.C. Fan, D.Y. Zheng, Stability of a cracked Timoshenko beam column by modified Fourier series, *Journal of Sound and Vibration* 264 (2003) 475–485.

[16] J.M. Chandra Kishen, A. Kumar, Finite element analysis for fracture behavior of cracked beam-columns, *Finite Elements in Analysis and Design* 40 (2004) 1773–1789.
[17] C.Y. Wang, C.M. Wang, T.M. Aung, Buckling of a weakened column, *Journal of Engineering Mechanics-ASCE* (11) (2004) 1373–1376.
[18] B. Binici, Vibration of beams with multiple open cracks subjected to axial force, *Journal of Sound and Vibration* 287 (2005) 277–295.
[19] J.D. Aristizabal-Ochoa, Timoshenko beam-column with generalized end conditions and nonclassical modes of vibration of shear beams, *Journal of Engineering Mechanics-ASCE* 130 (10) (2004) 1152–1159.
[20] S.P. Timoshenko, J.M. Gere, *Theory of Elastic Stability, Engineering Societies Monographs*, McGraw-Hill Book Company, New York, 1961.
[21] I.A. Karnovsky, O.L. Lebed, *Formulas for Structural Dynamics: Tables, Graphs and Solutions*, McGraw-Hill, New York, 2001.
[22] F. Engesser, Buckling resistance of straight bars, *Zentralblatt des Bauverwaltung, Issue* 11 (1889) 483 (in German).
[23] D.Y. Zheng, S.C. Fan, Vibration and stability of cracked hollow-sectional beams, *Journal of Sound and Vibration* 267 (2003) 933–954.
[24] SAP2000, version 6.1, *SAP2000 Integrated Finite Element Analysis and Design of Structures*, Computers and Structures, Inc., 1995 University Ave., Berkeley, CA 94704, USA, 1997.
[25] J.D. Aristizabal-Ochoa, Discussion of "Tension buckling in multilayer elastomeric bearings," *Journal of Engineering Mechanics-ASCE* 131 (1) (2005) 106–108.
[26] T.M. Roberts, Influence of shear deformation on buckling of pultruded fiber reinforced plastic profiles, *Journal of Composites for Construction-ASCE* (11) (2002) 241–248.
[27] J.D. Aristizabal-Ochoa, Static and dynamic stability of uniform shear buildings under generalized boundary conditions, *Journal of Sound and Vibration* (2007), accepted for Publication.
[28] Z.P. Bazant, Shear buckling of sandwich, fiber-composite and lattice columns, bearings and helical springs: paradox resolved, *Journal of Applied Mechanics-ASME* 70 (2003) 75–83.
[29] J.M. Kelly, Tension buckling in multilayer elastomeric bearings, *Journal of Engineering Mechanics-ASCE* 129 (12) (2003) 1363–1368.
[30] V. Nagaraj, H.V.S. Ganga Rao, Static behavior of pultruded GFRP beams, *Journal of Composites for Construction-ASCE* 1 (3) (1997) 120–129.